Review of spectral and polarization imaging systems

Sumera Sattar, Pierre-Jean Lapray, Alban Foulonneau, Laurent Bigué

Review of spectral and polarization imaging systems

Sumera Sattar[a], Pierre-Jean Lapray[a], Alban Foulonneau[a], and Laurent Bigué[a]

[a]Université de Haute-Alsace, IRIMAS UR 7499, F-68100 Mulhouse, France

ABSTRACT

Spectral and Polarization Imaging (SPI) is an emerging sensing method that combines the acquisition of both spectral and polarization information of a scene. It could benefit for various applications like appearance characterization from measurement, reflectance property estimation, diffuse/specular component separation, material classification, etc. In this paper, we present a review of recent SPI systems from the literature. We propose a description of the existing SPI systems in terms of technology employed, imaging conditions, and targeted application.

Keywords: spectral imaging, polarimetric imaging

1. INTRODUCTION

Conventional color imaging systems acquire images using three bandpass filters, commonly called R, G, and B, to constitute a color vector for a given point in a scene. The spectral sensitivity of color sensors exhibits peaks close to the wavelength bands that the human can perceive. It is therefore not well adapted to sample accurately the spectral power distribution of light, as it suffers from a lake of spectral resolution.[1] When accurate reflectance information from a surface is needed, MultiSpectral Imaging (MSI – Table 1 shows all the acronyms in the paper) or HyperSpectral Imaging (HSI) are preferred. The difference in terminology between MSI and HSI is rather fuzzy, but is relative to the spectral resolution of the system (i.e. number of spectral channels) for a given range of wavelengths. HSI typically has a high spectral resolution, that could lead to a better spectral reconstruction compared to MSI, but is still an expensive technique mainly encountered in remote sensing applications.[2] Even if some HSI technologies permit to capture the information in a snapshot way, it suffers from a lake of spatial resolution due to the number of spectral channels considered. MSI is a trade-off,[3,4] which is better suited for a wider application panel, like medical imaging,[5] food safety and quality,[6] or remote sensing.[7]

The polarization property of light complements the intensity and frequency light attributes. It conveys information about the orientation of the transverse electric fields that compose the electromagnetic radiation. Light could be unpolarized, partially, or fully polarized, and the polarization type could be characterized as linear, circular, or elliptical. Linear polarization is produced when the electric field oscillates in a single plane along the direction of propagation. Circular or elliptical polarization result from a phase shift between the two electric field components, resulting in a rotation of the electric field in the direction of propagation. Polarization analysis is exploited to characterize polarization or depolarization effects induced by either the reflection or transmission phenomenons. Polarization imaging permitted to retrieve surface reflectance properties for isotropic objects, like surface normals, index of refraction, specular component, etc. It also allowed to enhance some computational imaging algorithms like for dehazing[8] or contrast enhancement.[9]

Some biological organisms have strong vision capability and combine both spectral and polarization perception. Dragonfly or mantis shrimp are some of these; they develop the ability to detect and catch their prey, by revealing hidden or camouflaged surfaces.[10] Nowadays, mixing Spectral and Polarimetric Imaging (SPI) is an active emerging research area. For a more complete acquisition system, different research works have been carried out to explore the benefits of acquiring polarimetric images at different wavelength bands. The aim is to measure the intensity of the light using conventional or ad hoc imaging sensors coupled with several active and/or passive polarization optical elements. The output is a registered datacube containing multiple spectral

Further author information: (Send correspondence to S.S.)
S.S.: E-mail: sumera.sattar@uha.fr

bands and various polarization channels. Thus, a more complete measurement of surface characteristics becomes possible.

SPI systems can be classified using several imaging configurations, such as the ability to acquire sequentially or simultaneously the channels, the spatial/spectral resolutions, or the optical path configuration. It is of interest to review such aspects in order to help for further theoretical or experimental investigations. To this end, we propose to review and discuss the SPI imaging systems from the last decades.

The remainder of this paper is organized as follows. In Section 2, we first enunciate the basic models of spectral and polarization imaging, along with the definitions of the measurement conditions. Then, we propose a classification of SPI technologies in Section 3. Section 4 describes the applications that take benefits from SPI. Finally, a conclusion is provided in Section 5.

AOTF	Acousto-Optical Tunable Filter
CCD	Charge-Coupled Device
DMD	Digital Micro-mirror Device
DOA	Division Of Amplitude
DOFP	Division Of Focal Plane
DOP	Degree Of Polarization
DOT	Division Of Time
FRCI	Filter Rotation and/or Controlled Illumination
HSI	HyperSpectral Imaging
LCTF	Liquid Crystal Tunable Filter
LCVR	Liquid-Crystal Variable Retarder
LWIR	Long-Wave InfraRed
MSI	MultiSpectral Imaging
MWIR	Mid-Wave InfraRed
NIR	Near-InfraRed
PEM	Photo Elastic Modulator
PFA	Polarization Filter Array
PG	Polarization Grating
PSA	Polarization State Analyzer
SPI	Spectral and Polarization Imaging

Table 1. List of acronyms used in the paper, sorted by alphabetical order.

2. BACKGROUND AND DEFINITIONS

We first enunciate the most commonly used imaging models from both spectral and polarization imaging independently.

2.1 Spectral imaging model

Considering that a spectral imaging system could be modeled by a linear optoelectronic transfer function, the output response is relative to the integration of all the energy that reaches the sensor weighted by the sensitivities of each spectral band. All the optical elements have a non-perfect spectral transmission factor, all contributing

to the global system sensitivity. Assuming a linear and already noise-corrected system output, the response is represented by the following equation:

$$\rho_i = \int_{\lambda_{min}}^{\lambda_{max}} E(\lambda)R(\lambda)O(\lambda)C_i(\lambda)d\lambda \ , \tag{1}$$

where ρ_i is the response of the i'th spectral channel, $E(\lambda)$ is the spectral emission of the illuminant, $R(\lambda)$ is the spectral reflectance, $O(\lambda)$ is the global transmittance of all the optical elements, and $C_i(\lambda)$ is the spectral sensitivity of the i'th channel. λ_{max} and λ_{min} represent the boundings of the effective spectral range of the system.

The spectral behavior of elements from the factor $E(\lambda)O(\lambda)C_i(\lambda)$ are often partially or inaccurately known, or some of them may change over time. A typical assumption which is done is that the spectral power distribution of the illuminant and the spectral behavior of the optics are fixed. From this model, spectral reflectance could be recovered using a spectral reconstruction method.

The previous model is often enhanced by using the dichromatic model, either in the color[11] or spectral domain,[12] which considers a linear combination of the object spectral property and the highlight spectral property. Thus, the reflection has two components: a diffuse part and a specular part, which result respectively from a subsurface interaction and a surface interaction. The diffuse part is often assumed to be unpolarized, and the specular part to be totally or partially polarized (depending on the angle of incidence, the viewing angle, and the phase angle).

2.2 Polarization imaging model

The Stokes vector[13] $\mathbf{S}$ represents the state of polarization of the light at a given wavelength. It is the most common polarization formalism, and allows the partially and fully polarized light representation. The four components (i.e. the Stokes components) of the vector are derived from a set of intensity measurements of polarization components. Polarizing optical elements are located between the input light beam and a radiometer (i.e. an image sensor); this forms a Polarization State Analyzer (PSA). It is therefore possible to estimate the Stokes vector:

$$\mathbf{S} = \begin{bmatrix} s_0 \\ s_1 \\ s_2 \\ s_3 \end{bmatrix} = \begin{bmatrix} I_0 + I_{90} \\ I_0 - I_{90} \\ I_{45} - I_{135} \\ I_r - I_l \end{bmatrix} \ , \tag{2}$$

with s_0 the total light intensity, s_1 the difference between intensities measured through a 0° and 90° polarizers, s_2 the difference of intensities through a 45° and −45° polarizers, and s_3 the difference of intensities through a right and left circular polarizers.

The polarization-altering properties of an optical element or an object is mathematically represented using the Mueller formalism. Reflection, scattering, or transmission could change the state of polarization of an incident light beam. These changes are characterized by these optical parameters: depolarization, diattenuation, and retardance, which depend on space, time, and wavelength. After a light interaction, an input Stokes vector $\mathbf{S}$ is then transformed into an output Stokes vector $\mathbf{S}'$ as follows:

$$\mathbf{S}' = \mathbf{M}\mathbf{S}. \tag{3}$$

The 4×4 transformation matrix $\mathbf{M}$ is called the Mueller matrix.

A PSA is characterized by its analyzer vector $\mathbf{A} = [a_0 \ a_1 \ a_2 \ a_3]^T$, i.e. the first row of the Mueller matrix, which transforms the input Stokes vector $\mathbf{S}$ into a single camera response I (assuming no noise) such as:

$$I = \mathbf{A}\mathbf{S}. \tag{4}$$

Thus, the analyzer vector is a Stokes-like vector, which mentions the polarization state that produces the maximal response for the sensor. Now considering N measurements taken from different polarization analyzers, and assuming that the input Stokes vector is uniform, we could write:

$$\mathbf{I} = \begin{bmatrix} I_1 \\ I_2 \\ ... \\ I_N \end{bmatrix} = \mathbf{WS} = [\mathbf{A_1}\ \mathbf{A_2}\ \mathbf{A_3}\ ...\ \mathbf{A_N}]^T \begin{bmatrix} s_0 \\ s_1 \\ s_2 \\ s_3 \end{bmatrix}. \tag{5}$$

Number of acquisitions needed, along with the selection of the angle of analysis have been previously discussed by Tyo *et al.*[14] Angles could differ from the ones used to calculate the Stokes vector in Eq. 2, and polarization elements do not need to be ideal, thus the polarimeter has to be polarimetrically calibrated[15–17] by estimating $\mathbf{W}$. Afterward, $\mathbf{S}$ can be deduced by an inversion procedure, and polarization properties of light beams like Angle Of Linear Polarization (AOLP), Degree Of Polarization (DOP), or ellipticity, can be derived from the Stokes vector.

2.3 Measurement considerations

All the technologies presented in the following Section have several compromises on their imaging capacities, in terms of spatial and spectral resolution, spectral range, estimation of polarization properties, or lightning patterns.

Some devices exhibit Instantaneous Field of View (IFOV) errors[18] because a single pixel of a camera only senses a fraction of the total spectral/polarization channels available, so the missing spatial information by pixel position has to be interpolated to recover the full spatial resolution.[19,20] This problem is generally encountered in many filter array imaging devices,[3,19] as different channels are spatially distributed on the focal plane of the sensor. In this case, the spectral resolution also determines the spatial resolution, as the spectral data cube is more dispersed with a high spectral resolution (i.e more channels). This phenomenon is even more pronounced as the number of channels is large.

Selection of spectral characteristics of SPI is often task-specific, and is addressed during the system specification. One can differentiate three types of spectral characteristics: the spectral range of interest, the number of channels in the spectral range considered, and the bandwidth (i.e. the full-width at half-maximums parameter). It offers large design possibilities in terms of spectral sensitivities. The spectral range can be part or a mix of the visible (VIS), near-infrared (NIR), short-wave infrared (SWIR), mid-wave infrared (MWIR), or long-wave infrared (LWIR). Some applications used spectral channels that are often equally-spaced in the spectral range considered, with a defined spectral increment. The greater the number of bands present in the wavelength range considered, the better the spectral resolution. For example, Alouini *et al.*,[9] Bartlett *et al.*,[21] and Bishop *et al.*[22] use respectively 5, 10, and $50nm$ for the spectral increment, over a spectral range of respectively $800-2100nm$, $450-720nm$, and $600-850nm$. Polarimetrically speaking, it has been found that polarization signatures[23] in the visible and NIR parts of the spectrum are dominated by reflection. Goldstein *et al.*[24] first explored the Stokes behavior of several targets in the visible and near-infrared to highlight the interest of analyzing polarization signatures spectrally.

Lot of practical polarimeters are designed only for recovering the linear polarization states of the light. Nevertheless, some recent works argue that, especially for dielectrics, a non-negligible fraction of light is circularly polarized after the reflection of unpolarized light.[25] Circular polarization is relatively more difficult to capture than purely linear polarization in SPI systems, as it needs circular polarizing elements in the PSA (e.g. quarter-waveplates), that have polarization properties which vary with wavelength (i.e. retardance).

Another consideration is the spectral interpretation of polarization signatures. The reflection of light over a surface induces a particular polarization effect (relatively to the plane of incidence), which is described by the Fresnel reflection coefficients.[26] These coefficients are function of the refractive indexes of the two media that compose the reflection interface, and are complex number depending on wavelength. Thus, polarization state of light is wavelength dependent. Strictly speaking, a unique Stokes vector $\mathbf{S}(\lambda)$ should be computed by wavelength. Some works assume that this dependency is negligible when operating in the visible wavelength range,[27] i.e.

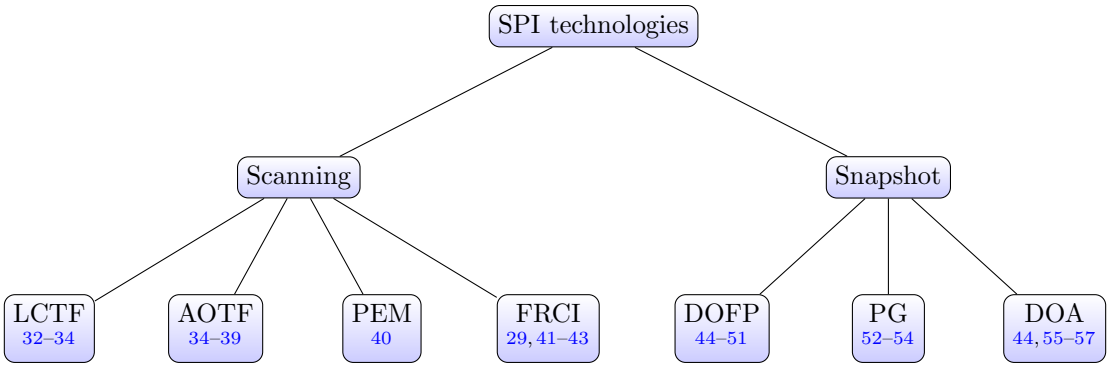

Figure 1. Proposed classification of SPI.

the Stokes vectors are constant. Other works[28,29] consider that the wavelength-dependency is negligible per spectral channels, which makes it possible to more precisely discriminate the amplitude of polarization over the wavelengths.

Lightning geometry (i.e. incidence angle, viewing angle) has an impact on the dynamic range of intensities that reach the PSA sensor. For example, dielectric materials have small polarization signatures when viewed near to the object normal. This can cause application failure due to low intensity contrasts which are below the noise level of the sensor. Moreover, when the angles of incidence come to vary greatly (and up to the Brewster angle), the high dynamic range of intensities generated makes it impossible for the sensor to distinguish both weak and strong polarization signatures. Nowadays, as dynamic range of imaging sensors and computational imaging algorithms[30] have been enhanced, these problems can be reassessed, and distinguishing small polarization signatures near to the normal, or over different close wavelength ranges, becomes more feasible practically.

3. SPECTRAL AND POLARIZATION IMAGING TECHNOLOGIES

Polarimeters and spectral cameras are commonly classified into two main categories: scanning and snapshot techniques. All Division-Of-Time (DOT) polarimeters belong to the scanning techniques, as multiple images are captured sequentially to recover the polarization information. Division Of Amplitude (DOA) and Division Of Focal Plane (DOFP) devices are parts of the snapshot techniques, which aim to perform a one-shot acquisition. Recent reviews[3,31] about existing polarimeters and spectral imaging systems have been done separately, and we believe that SPI systems could also be examined in the same way. Thus, we review recent SPI technologies and present a classification in Figure 1, and a technical description summary in Table 2.

3.1 General approach

On a basic level, all SPI systems consist of polarizers, spectrally-selective optical elements, and an image sensor (either CCD or CMOS). SPI specifications include the spectral resolution, the spectral range, the spatial resolution, or the polarimetric analyzing capability, i.e. Stokes or Mueller.

3.2 Scanning SPI

Division-Of-time (DOT) SPI systems are scanning techniques composed of spectrally selective elements and a polarimeter. At different time slots, the spectral sensitivity is changed or tuned in some way to acquire a new image. In the DOT systems, both image scene and acquisition system must be static, because any movement during acquisition produces artifacts and results in blurring effects. First DOT systems were slow. To increase the system speed, evolved tunable filters have been manufactured, like the LCTFs, AOTFs, and PEMs. We discuss several DOT setups below.

Reference	Polarization Mode	Sensing Instruments	Illumination	Spectral Range	Spectral Bands
Scanning					
Alouini *et al.*[9,54]	DOLP	LP, push broom hyperspectral imager	A or P - Polarized optical pulses at 5 wavelengths	800nm - 2200nm	256
Bishop *et al.*[22]	Full-Stokes	Rotated QWP, LP	A or P	600nm - 850nm	4
Ma *et al.*[29]	Fresnel coefficients	LP or CP	A - Sphere of 156 polarized (with LP or CP) LED	VIS	3
Lapray *et al.*[41]	Linear-Stokes	2 LPs, bandpass filters, 2-CCD prism camera	P - Tungsten-filament lamp	VIS, NIR	6
Yu *et al.*[43]	Full-Stokes	LP, QWP	P - 3 laser light sources at 450nm, 532nm, and 633nm	VIS	3
Kurosaki *et al.*[32]	-	Rotated LCTF	P	VIS	7
Homma *et al.*[33]	Polarization states	Rotated LCTF	P	650nm-1100nm	10
Qi *et al.*[34]	Full-Stokes	PFA, LCVR	A - Narrowband halogen light source	VIS	2
Riviere *et al.*[58]	Stokes	LP	P - Uncontrolled illumination	VIS	3
Ghosh *et al.*[59]	Full-Stokes	LP, CP	A - Sphere of 150 circularly polarized LED	VIS	3
Ghosh *et al.*[60]	Fresnel coefficients	LPs	A - Sphere of 150 linearly polarized LED, LCD monitor, Projector	VIS	3
Pierangelo *et al.*[61]	Mueller	LP, LCTF, bandpass filters	A - Halogen Source	500nm-700nm	5
Bartlett *et al.*[62]	Linear-Stokes	4-LPs, 6 bandpass filters	P	VIS, NIR	10
Fyffe *et al.*[63]	Fresnel coefficients	Polarizing beam splitter, LPs	A - 3 LED sphere	VIS	3
Snapshot					
Tu *et al.*[44]	Full-Stokes	LPs	A or P - Broadband illumination	VIS	3
Li *et al.*[55]	Full-Stokes	2 birefringent crystal retarders, LP, WP	A or P - Uniform light source sphere	450nm-1000nm	12
Zhang *et al.*[57]	Full-Stokes	LP, WP, Savart polariscope	P - Polychromatic uniform light	VIS	-
Kulkarni *et al.*[45], **Garcia *et al.*[46]**	Linear-Stokes	PFA, Foveon's vertically stacked photodetectors	P	VIS	3
Fu *et al.*[49]	Linear-Stokes	PFA, rotated prism	A - Unpolarized illumination	505nm-650nm	8
Kim *et al.*[52,53]	Full-Stokes	Polarization gratings, QWP	A - Monitor	500nm – 700nm	51
Thilak *et al.*[64]	DOP	-	P - Uncontrolled illumination	VIS	-
Mu *et al.*[56]	Linear-Stokes	PFA, optical mask with slits, dispersing prism	A- Polychromatic light	450nm-650nm	3
Soldevila *et al.*[65]	Linear-Stokes	Digital micro-mirror device DMD	A - Broadband illumination	490nm-660nm	7

Table 2. Works using SPI systems and technologies. Acronyms: A (Active polarization system), QWP (Quarter-WavePlate), P (Passive polarization system), WP (Wollaston Prism), LP (Linear Polarizer), and CP (Circular Polarizer).

3.2.1 Filter Rotation and/or Controlled Illumination (FRCI)

Lapray *et al.*[41] proposed an SPI system based on filter rotation. A dual-sensor camera operates in the visible and the near-infrared parts of the spectrum. It is combined with two linear polarization filters: one operating

efficiently in the visible, and one in the near-infrared. The polarization filters are mounted in two motorized rotational stages and the dual-RGB method[42] is employed to generate 6 different spectral bands from a spectral recombination of two bandpass filtered RGB images.

Time-multiplexed controlled illumination is another scanning technique for spectral modulation or spatial modulation (viewpoint dependent measurements). A practical full-Stokes setup using laser source[43] has been demonstrated to recover all of the four Stokes components at three specific wavelengths. It contains a linear polarizer, a rotating quarter-waveplate, three laser sources (432, 532, and 633nm), and a CCD sensor. The Stokes reconstruction is done with very narrow wavelength bands. Such a system is adequate for task-specific applications that require accurate polarization measurement on pre-selected wavelengths.

Ma *et al.*[29] explored an acquisition setup that consists of an RGB camera, and a set of linear or circular polarizers combined with a polarized (linear or circular) LED-based spherical illumination. Spherical gradient patterns are sequentially emitted to generate several incident illumination angles. They show that diffuse and specular component separation could be done by either using linear or circular polarization. Moreover, based on the assumption that there is usually a skew in the derived normal directions from non-separated components, they compute the normal maps per color channel, and per specular and diffuse components independently. It appears that shorter wavelengths (blue channel), along with the use of specular channel, is the best combination to recover the details about the surface.

3.2.2 Liquid Crystal Tunable Filters

The Liquid Crystal Tunable Filter (LCTFs) transmits the light within a specific wavelength band, whose effective transmission is done by changing the electrical voltage at the input. It is also an addressable polarization modulator, which can benefit from the birefringent properties of the liquid crystal cells. For about 20 years, liquid crystal cells have been incorporated into polarimeters, allowing measurements to be made at a higher rate compared to the manual or motorized filter rotation procedure.

Kurosaki *et al.*[32] proposed two LCTF prototypes which acquire spectral polarization information by continuously varying wavelength and polarization angle by rotating the LCTF through stepping motor or manual. Homma *et al.*[33] also proposed LCTF SPI system based on stepping motor to rotate the LCTF in the range of -90 to $+90$ degrees. A real-time full Stokes SPI system is explored by Qi *et al.*,[34] where a Liquid Crystal Variable Retarder (LCVR) is stacked over a linear DOFP polarimeter to capture the full-Stokes vector. They calibrate and characterized the system for two specific narrow wavelength-bands, corresponding to the optimum retardance states of their LCVR, but the system can be adapted to the desired band and is able to capture the images in real-time.

3.2.3 Acousto-Optic Tunable Filters

Another kind of device, with different advantages in comparison with the LCTF, is the Acousto-Optic Tunable Filters (AOTFs). It is composed of tellurium oxide or quartz optical tunable filter. These birefringent crystals vary their response to an applied acoustic field, so that the incoming light that hits the gratings is diffracted within a given sound wave, resulting in a shift of the spectral frequency. Compared to the manual or automatic filter rotation procedure, the wavelength transition of these filters is much faster, which leads to rapid access to the spectral bands. For comparison with LCTF, AOTF is less easy to use, has less spatial resolution, but has superior spectral resolution and switching capability.[35] Gupta *et al.*[36] achieve full-Stokes imaging by using an LCVR for the polarization analysis, in conjunction with an AOTF.

The AOTF based spectral imaging systems proposed by Sturgeon *et al.*[37] uses two diffracted orthogonal polarized band images simultaneously with two separate image detectors. Glenar *et al.*,[38] Li *et al.*,[39] and Qubta *et al.*[36] proposed AOTF-based systems which use only one image detector and an external variable retarder in front of the AOTF to alter the input light polarization. Qi *et al.*[34] explored an hybrid system with both AOTF and DOFP technologies, that uses DOFP camera to measure the linear Stokes parameters in a snapshot way.

3.2.4 Photo Elastic Modulators

The photo-detector in PEM is an extremely sensitive photomultiplier tube, which is capable to acquire polarization measurements in the wide spectral range. Photo Elastic Modulators (PEMs) are suitable for a high sensitivity of polarization sensing. In works by Diner *et al.*,[40] a PEM is a polarizing element, whereas a diffraction grating permits to select the spectral sensitivity of the system.

3.3 Snapshot SPI

3.3.1 Division Of Amplitude

A DOA polarimeter splits the incident light into different optical paths, each path associated with a separate imaging sensor. A traditional way is to employ a prism as a splitting element. This kind of device needs an accurate geometric calibration and a registration step that is usually difficult to achieve. The imaging setup is also often big to accommodate for the optical paths.

A few research works have coupled DOFP (see next Section) and DOA principles. The aim is to upgrade a DOFP to a full-Stokes snapshot camera, by including additional optical devices in the optical path. Tu *et al.*[44] is one of these works. They combine two RGB DOFP cameras (equipped with linear micro-polarizers and Bayer filters), where the incoming light is divided into two beams by a non-polarizing cube beam splitter. One camera is combined with a quarter-waveplate to capture the circular polarization state of light, whereas the other is sensing the linear states. Alignment of the two division of focal plane cameras is therefore cumbersome, and data need to be calibrated carefully, polarimetrically and spectrally. In another manner, Mu *et al.*[56] used a channeled spectropolarimetry technique to acquire linear polarization information in the RGB channels. The optical path is arranged so that the light is splitted spatially by rectangular slits, and splitted spectrally by a dispersive element. A DOFP camera recovers the generated dispersed patterns with four polarization angles of analysis, and a channeled demodulation is then employed to recover a sparse polarization and spectral datacube. The DOA configuration remains in the fact that a second camera (RGB) is employed in parallel. It gives RGB images of the same scene within a high spatial resolution, to assist the post-processing for obtaining the full spatial resolution of the datacube.

Fourier-transform imaging spectropolarimeter using Wollaston prism interferometer has also been studied.[55,57,66] They can be considered as DOA systems as the incoming light is splitted into different beams. The advantages of these techniques is their relative compactness, and the absence of moving parts or electrically controllable devices. Nevertheless, they require numerical inversion procedures that are computationally expensive, and are not suited for images containing low spatial frequencies and/or high spectral frequencies.[23]

3.3.2 Division Of Focal Plane

Color and linear-polarization snapshot SPI system have been investigated in ad hoc sensor designs, which employ the Foveon's vertically stacked process.[45,46] These sensors are one-shot, compact, and could potentially be embedded into flexible endoscopes. They could also recover the spectral information by pixel without the need of prior spatial interpolation. Nevertheless, spectral resolution is often weak, containing wide spectral bands with a lot of spectral overlap.

The IMX250 MYR Sony sensor[47] is composed of two filter arrays: a Polarization Filter Array (PFA), and a Bayer-like filter, one above the other. The Quad-Bayer spatial arrangement is employed for RGB filtering, and is coupled with the most common micro-polarizer arrangement.[48] In comparison with the Foveon hardware architecture, this technique has the advantage of using conventional sensors, and has less spectral overlap between channels. Because a single pixel capture only one of the 12 channels at one particular position, this method suffers from instantaneous field of view artefacts, and thus needs a dedicated spatial interpolation to recover the full resolution of the image, i.e. the demosaicing process. A complementary approach using PFA and colored patterned detector was also developed by Fu *et al.*[49] The DOFP is combined with a rotated prism (so no more snapshot at all) to disperse the light and achieve better spectral reconstruction compared to a single snapshot.

Other works deal with intrinsic circular polarization sensing embedded in custom polarization filter arrays. It uses either liquid crystal polymer micro-polarizers,[50] or chiral transmission structures[51] (plasmonic nanoantennas) as circular polarization filters. These devices can theoretically sense the polarization in a snapshot way,

and have the full-Stokes capability. They could potentially be adapted to several but limited spectral bandwidth. Nowadays, they are generally difficult to manufacture.

3.3.3 Polarization Grating

Most methods for joint acquisition require modulation processes and moving parts that reduce sampling resolution and have significant complexity. To overcome these limitations, anisotropic diffraction gratings called Polarization Grating (PG) have been implemented[52–54] to separate chromatic and polarization information spatially. PG has the property to generate chromatic dispersion that is proportional to the polarization state of light. Thus, polarization diffraction causes dispersion of the light beam, generating patterns which can be focused on a focal plane array and captured. Additional combinations of PGs and wave-plates permit to generate different dispersion patterns, leading to different polarization properties to be recovered. This technique has the advantage of capture information at high spectral resolution ($\approx 1nm$), and has the snapshot capability within a simple and compact design.

4. IMAGING APPLICATIONS

SPI is used in the literature for surface reflectance characterization. It includes the separation of diffuse and specular components,[27] the index of refraction estimation,[64,67,68] the surface normal reconstruction,[29,69] or the specular roughness estimation.[60] These reflectance parameters are relatively difficult to estimate accurately within a single lightning condition; one need some cumbersome imaging configurations. For example, spatially controlled lightning environment are needed, like spherical gradient illumination,[29] uniform spherical field of circularly polarized illumination,[59] or second order spherical gradient illumination patterns.[60] Recently, Riviere *et al.*[58] extract a complete set of surface reflectance parameters for planar surfaces from an uncontrolled lightning environment. They use a single camera combined with a rotated linear polarizer. A set of three linear polarization images are captured at three viewpoints: one near orthogonal, and two close to the Brewster angle. Moreover, active diffuse polarization[69] is used to estimate jointly the surface orientation and the refractive index. An adaptation of this was done specifically for dielectric objects and proposed by Huynh *et al.*[67]

Surveillance, recognition, and tracking[21,70] are applications that take advantage of spectral and polarization imagery, using prior knowledge about the spectral and polarization signatures of targets. It helps to distinguish the man-made objects, especially in low contrast conditions, e.g. hidden or camouflaged targets.

The tissue birefringence and structures are changed by pathologies. The reflectance variation in skin, which can be measured by the SPI,[71,72] has proved to be a powerful diagnostic tool to isolate pathology features.[73] For example, due to their structures, it has been found that the degree of dehydration is linked with the polarization signature (in the Mueller formalism) of biological tissues.[34] Detecting residual cancer is another application. For example, after neoadjuvant treatment, contrast enhancement using polarization images permits for detecting residual tumors in rectum samples.[61] It is done by Mueller imaging, where depolarization is analyzed at different wavelengths to have sufficient qualitative information to have enough detection sensitivity. Another medical application among many is the monitoring of mineral loss and tooth decay.[74]

Spectral polarization imaging also plays an effective role in critical weather or underwater conditions.[8,75,76] Due to light scattering by particles, a polarization signature is generated and can be physically modeled. Thus, it is then possible to deduce the size, density, and distribution of the suspended particles, and correct the image by imaging model inversion.

Finally, some SPI systems have been utilized in remote sensing applications, to discriminate plant species, detect forest,[77] or detect icy objects.[32] With the distinction of polarization and spectral data reflected by sand, soil, or water, multi-band polarization imaging uncovers the critical data to analyze landforms and geography.

5. CONCLUSION

We reviewed the papers from the literature that deal with both polarimetric and spectral imaging. Scanning and snapshot imaging setups are the two main categories of SPI systems. Nowadays, snapshot sensors with both polarization and RGB capability are coming on the market and become out-of-the-lab instruments. The SONY IMX253 MYR sensor[47] is one of the promising solutions, where the division of focal plane sensors are composed

by multiple patterned filter layers over the sensor. The technology could potentially be a solution for future application demands, offering large capabilities in terms of acquisition frame rate, resolution, polarization accuracy, and versatility. It could also be a good instrument for validation of imaging models for future computational imaging algorithm development.

Acknowledgment

This work was supported by the ANR JCJC SPIASI project, grant ANR-18-CE10-0005 of the French Agence Nationale de la Recherche.

REFERENCES

[1] Shrestha, R., Hardeberg, J. Y., and Mansouri, A., "One-shot multispectral color imaging with a stereo camera," in [*Digital Photography VII*], **7876**, 787609, International Society for Optics and Photonics (2011).

[2] Sattar, S., Khan, H. A., and Khurshid, K., "Optimized class-separability in hyperspectral images," in [*2016 IEEE International Geoscience and Remote Sensing Symposium (IGARSS)*], 2711–2714, IEEE (2016).

[3] Lapray, P.-J., Wang, X., Thomas, J.-B., and Gouton, P., "Multispectral filter arrays: Recent advances and practical implementation," *Sensors* **14**(11), 21626–21659 (2014).

[4] Thomas, J.-B., Lapray, P.-J., Gouton, P., and Clerc, C., "Spectral characterization of a prototype sfa camera for joint visible and nir acquisition," *Sensors* **16**(7) (2016).

[5] Ewerlf, M., Larsson, M., and Salerud, E. G., "Spatial and temporal skin blood volume and saturation estimation using a multispectral snapshot imaging camera," in [*Imaging, Manipulation, and Analysis of Biomolecules, Cells, and Tissues XV*], Farkas, D. L., Nicolau, D. V., and Leif, R. C., eds., **10068**, 105 – 116, International Society for Optics and Photonics, SPIE (2017).

[6] Qin, J., Chao, K., Kim, M. S., Lu, R., and Burks, T. F., "Hyperspectral and multispectral imaging for evaluating food safety and quality," *Journal of Food Engineering* **118**(2), 157–171 (2013).

[7] Huang, Y., Thomson, S. J., Lan, Y., and Maas, S. J., "Multispectral imaging systems for airborne remote sensing to support agricultural production management," *International Journal of Agricultural and Biological Engineering* **3**(1), 50–62 (2010).

[8] Schechner, Y. Y., Narasimhan, S. G., and Nayar, S. K., "Instant dehazing of images using polarization," in [*CVPR (1)*], 325–332 (2001).

[9] Alouini, M., Goudail, F., Grisard, A., Bourderionnet, J., Dolfi, D., Baarstad, I., Løke, T., Kaspersen, P., and Normandin, X., "Active polarimetric and multispectral laboratory demonstrator: contrast enhancement for target detection," in [*Electro-Optical Remote Sensing II*], **6396**, 63960B, International Society for Optics and Photonics (2006).

[10] Horváth, G., Horváth, G., Varju, D., and Horváth, G., [*Polarized light in animal vision: polarization patterns in nature*], Springer Science & Business Media (2004).

[11] Shafer, S. A., "Using color to separate reflection components," *Color Research & Application* **10**(4), 210–218 (1985).

[12] Tominaga, S. and Wandell, B. A., "Standard surface-reflectance model and illuminant estimation," *J. Opt. Soc. Am. A* **6**, 576–584 (Apr 1989).

[13] Stokes, G., "On the composition and resolution of streams of polarized light from different sources," *Transactions of Cambridge Philosophical Society* **9**, 339–416 (1852).

[14] Tyo, J. S., "Optimum linear combination strategy for an n-channel polarization-sensitive imaging or vision system," *J. Opt. Soc. Am. A* **15**, 359–366 (Feb 1998).

[15] LaCasse, C. F., Tyo, J. S., and Chipman, R. A., "Role of the null space of the drm in the performance of modulated polarimeters," *Opt. Lett.* **37**, 1097–1099 (Mar 2012).

[16] Giménez, Y., Lapray, P.-J., Foulonneau, A., and Bigué, L., "Calibration for polarization filter array cameras: recent advances," in [*Fourteenth International Conference on Quality Control by Artificial Vision*], Cudel, C., Bazeille, S., and Verrier, N., eds., **11172**, 297 – 302, International Society for Optics and Photonics, SPIE (2019).

[17] Giménez, Y., Lapray, P.-J., Foulonneau, A., and Bigué, L., "Calibration algorithms for polarization filter array camera: survey and evaluation," *Journal of Electronic Imaging* **29**(4), 1 – 13 (2020).

[18] Ratliff, B. M., LaCasse, C. F., and Tyo, J. S., "Interpolation strategies for reducing ifov artifacts in microgrid polarimeter imagery," *Opt. Express* **17**, 9112–9125 (May 2009).

[19] Mihoubi, S., Lapray, P.-J., and Bigué, L., "Survey of demosaicking methods for polarization filter array images," *Sensors* **18**(11) (2018).

[20] Qiu, S., Fu, Q., Wang, C., and Heidrich, W., "Polarization Demosaicking for Monochrome and Color Polarization Focal Plane Arrays," in [*Vision, Modeling and Visualization*], Schulz, H.-J., Teschner, M., and Wimmer, M., eds., 117–124, The Eurographics Association (2019).

[21] Bartlett, B. D., Schlamm, A., Salvaggio, C., and Messinger, D. W., "Anomaly detection of man-made objects using spectropolarimetric imagery," in [*Algorithms and Technologies for Multispectral, Hyperspectral, and Ultraspectral Imagery XVII*], **8048**, 80480B, International Society for Optics and Photonics (2011).

[22] Bishop, K. P., McIntire, H. D., Fetrow, M. P., and McMackin, L. J., "Multispectral polarimeter imaging in the visible to near ir," in [*Targets and Backgrounds: Characterization and Representation V*], **3699**, 49–57, International Society for Optics and Photonics (1999).

[23] Tyo, J. S., Goldstein, D. L., Chenault, D. B., and Shaw, J. A., "Review of passive imaging polarimetry for remote sensing applications," *Applied optics* **45**(22), 5453–5469 (2006).

[24] Goldstein, D. H., Chenault, D. B., Gulley, M. G., and Spradley, K. D., "Near-infrared imaging polarimetry," in [*Polarization Analysis and Measurement IV*], **4481**, 100–108, International Society for Optics and Photonics (2002).

[25] Guarnera, G. C., Peers, P., Debevec, P., and Ghosh, A., "Estimating surface normals from spherical stokes reflectance fields," in [*European Conference on Computer Vision*], 340–349, Springer (2012).

[26] Born, M., "Principles of optics," *Electromagnetic Theory of Propagation, Interference and Diffraction of Light* **808** (1965).

[27] Nayar, S. K., Fang, X.-S., and Boult, T., "Separation of reflection components using color and polarization," *International Journal of Computer Vision* **21**(3), 163–186 (1997).

[28] Shinoda, K., Ohtera, Y., and Hasegawa, M., "Snapshot multispectral polarization imaging using a photonic crystal filter array," *Optics express* **26**(12), 15948–15961 (2018).

[29] Ma, W.-C., Hawkins, T., Peers, P., Chabert, C.-F., Weiss, M., and Debevec, P., "Rapid acquisition of specular and diffuse normal maps from polarized spherical gradient illumination," in [*Proceedings of the 18th Eurographics conference on Rendering Techniques*], 183–194, Eurographics Association (2007).

[30] Lapray, P.-J., Thomas, J.-B., and Gouton, P., "High dynamic range spectral imaging pipeline for multispectral filter array cameras," *Sensors* **17**(6) (2017).

[31] Lapray, P.-J., Gendre, L., Foulonneau, A., and Bigué, L., "An fpga-based pipeline for micropolarizer array imaging," *International Journal of Circuit Theory and Applications* **46**(9), 1675–1689 (2018).

[32] Kurosaki, H., Koshiishi, H., Suzuki, T., and Tsuchiya, K., "Development of tunable imaging spectropolarimeter for remote sensing," *Advances in Space Research* **32**(11), 2141–2146 (2003).

[33] Homma, K., Shingu, H., Yamamoto, H., Shibayama, M., Sugahara, K., and Itano, S., "Agro-environment observation using near-infrared lctf spectropolarimeter," in [*Multispectral and Hyperspectral Remote Sensing Instruments and Applications II*], **5655**, 407–418 (2005).

[34] Qi, J., He, C., and Elson, D. S., "Real time complete stokes polarimetric imager based on a linear polarizer array camera for tissue polarimetric imaging," *Biomedical optics express* **8**(11), 4933–4946 (2017).

[35] Abdlaty, R., Sahli, S., Hayward, J., and Fang, Q., "Hyperspectral imaging: comparison of acousto-optic and liquid crystal tunable filters," in [*Medical Imaging 2018: Physics of Medical Imaging*], Lo, J. Y., Schmidt, T. G., and Chen, G.-H., eds., **10573**, 700 – 708, International Society for Optics and Photonics, SPIE (2018).

[36] Gupta, N., Dahmani, R., and Choy, S. J., "Acousto-optic tunable filter-based visible-to-near-infrared spectroploarimetric imager," *Optical Engineering* **41** (2002).

[37] Sturgeon, M. A., Cheng, L.-J., Durkee, P. H., Hamilton, M. K., Huth, J. F., Mahoney, J. C., Olsen, R. C., and Reyes, G. F., "Spectral and polarimetric analysis of hyperspectral data collected by an acousto-optic tunable filter system," in [*Algorithms for Multispectral and Hyperspectral Imagery*], **2231**, 167–176, International Society for Optics and Photonics (1994).

[38] Glenar, D. A., Hillman, J. J., Saif, B., and Bergstralh, J., "Acousto-optic imaging spectropolarimetry for remote sensing," *Applied Optics* **33**(31), 7412–7424 (1994).

[39] Li, F., Xu, Y., and Ma, Y., "Design of hyper-spectral and full-polarization imager based on aotf and lcvr," in [*International Symposium on Optoelectronic Technology and Application 2014: Imaging Spectroscopy; and Telescopes and Large Optics*], **9298**, 92980U, International Society for Optics and Photonics (2014).

[40] Diner, D. J., Davis, A., Hancock, B., Gutt, G., Chipman, R. A., and Cairns, B., "Dual-photoelastic-modulator-based polarimetric imaging concept for aerosol remote sensing," *Applied optics* **46**(35), 8428–8445 (2007).

[41] Lapray, P.-J., Gendre, L., Foulonneau, A., and Bigué, L., "Database of polarimetric and multispectral images in the visible and nir regions," in [*Unconventional Optical Imaging*], **10677**, 1067738, International Society for Optics and Photonics (2018).

[42] Imai, F. H. and Berns, R. S., "Spectral estimation of artist oil paints using multi-filter trichromatic imaging," in [*9th Congress of the International Colour Association*], **4421**, 504–507, International Society for Optics and Photonics (2002).

[43] Yu, M., Liu, T., Huang, H., Hu, H., and Huang, B., "Multispectral stokes imaging polarimetry based on color ccd," *IEEE Photonics Journal* **8**(5), 1–10 (2016).

[44] Tu, X., Spires, O. J., Tian, X., Brock, N., Liang, R., and Pau, S., "Division of amplitude rgb full-stokes camera using micro-polarizer arrays," *Optics Express* **25**(26), 33160–33175 (2017).

[45] Kulkarni, M. and Gruev, V., "Integrated spectral-polarization imaging sensor with aluminum nanowire polarization filters," *Optics express* **20**(21), 22997–23012 (2012).

[46] Garcia, M., Edmiston, C., Marinov, R., Vail, A., and Gruev, V., "Bio-inspired color-polarization imager for real-time in situ imaging," *Optica* **4**(10), 1263–1271 (2017).

[47] Sony, "Polarization image sensor," tech. rep., Polarsens (2018).

[48] Chun, C. S., Fleming, D. L., and Torok, E., "Polarization-sensitive thermal imaging," in [*Automatic Object Recognition IV*], **2234**, 275–286, International Society for Optics and Photonics (1994).

[49] Fu, C., Arguello, H., Sadler, B. M., and Arce, G. R., "Compressive spectral polarization imaging by a pixelized polarizer and colored patterned detector," *JOSA A* **32**(11), 2178–2188 (2015).

[50] Bachman, K. A., Peltzer, J. J., Flammer, P. D., Furtak, T. E., Collins, R. T., and Hollingsworth, R. E., "Spiral plasmonic nanoantennas as circular polarization transmission filters," *Opt. Express* **20**, 1308–1319 (Jan 2012).

[51] Hsu, W.-L., Myhre, G., Balakrishnan, K., Brock, N., Ibn-Elhaj, M., and Pau, S., "Full-stokes imaging polarimeter using an array of elliptical polarizer," *Opt. Express* **22**, 3063–3074 (Feb 2014).

[52] Kim, J. and Escuti, M. J., "Snapshot imaging spectropolarimeter utilizing polarization gratings," in [*Imaging Spectrometry XIII*], **7086**, 708603, International Society for Optics and Photonics (2008).

[53] Kim, J. and Escuti, M. J., "Demonstration of a polarization grating imaging spectropolarimeter (PGIS)," in [*Polarization: Measurement, Analysis, and Remote Sensing IX*], Chenault, D. B. and Goldstein, D. H., eds., **7672**, 80 – 88, International Society for Optics and Photonics, SPIE (2010).

[54] Alouini, M., Goudail, F., Grisard, A., Bourderionnet, J., Dolfi, D., Bénière, A., Baarstad, I., Løke, T., Kaspersen, P., Normandin, X., et al., "Near-infrared active polarimetric and multispectral laboratory demonstrator for target detection," *Applied optics* **48**(8), 1610–1618 (2009).

[55] Li, J., Gao, B., Qi, C., Zhu, J., and Hou, X., "Tests of a compact static fourier-transform imaging spectropolarimeter," *Optics express* **22**(11), 13014–13021 (2014).

[56] Mu, T., Pacheco, S., Chen, Z., Zhang, C., and Liang, R., "Snapshot linear-stokes imaging spectropolarimeter using division-of-focal-plane polarimetry and integral field spectroscopy," *Scientific reports* **7**, 42115 (2017).

[57] Zhang, C., Quan, N., and Mu, T., "Stokes imaging spectropolarimeter based on channeled polarimetry with full-resolution spectra and aliasing reduction," *Applied optics* **57**(21), 6128–6134 (2018).

[58] Riviere, J., Reshetouski, I., Filipi, L., and Ghosh, A., "Polarization imaging reflectometry in the wild," *ACM Transactions on Graphics (TOG)* **36**(6), 206 (2017).

[59] Ghosh, A., Chen, T., Peers, P., Wilson, C. A., and Debevec, P., "Circularly polarized spherical illumination reflectometry," *ACM Transactions on Graphics (TOG)* **29**(6), 162 (2010).

[60] Ghosh, A., Chen, T., Peers, P., Wilson, C. A., and Debevec, P., "Estimating specular roughness and anisotropy from second order spherical gradient illumination," in [*Computer Graphics Forum*], **28**(4), 1161–1170, Wiley Online Library (2009).

[61] Pierangelo, A., Manhas, S., Benali, A., Fallet, C., Totobenazara, J.-L., Antonelli, M. R., Novikova, T., Gayet, B., De Martino, A., and Validire, P., "Multispectral mueller polarimetric imaging detecting residual cancer and cancer regression after neoadjuvant treatment for colorectal carcinomas," *Journal of biomedical optics* **18**(4), 046014 (2013).

[62] Bartlett, B. D., Faulring, J. F., and Salvaggio, C., "System characterization and analysis of the multispectral aerial passive polarimeter system (mapps)," in [*Polarization Science and Remote Sensing V*], **8160**, 81600A, International Society for Optics and Photonics (2011).

[63] Fyffe, G. and Debevec, P., "Single-shot reflectance measurement from polarized color gradient illumination," in [*2015 IEEE International Conference on Computational Photography (ICCP)*], 1–10, IEEE (2015).

[64] Thilak, V., Voelz, D. G., and Creusere, C. D., "Polarization-based index of refraction and reflection angle estimation for remote sensing applications," *Applied Optics* **46**(30), 7527–7536 (2007).

[65] Soldevila, F., Irles, E., Durán, V., Clemente, P., Fernández-Alonso, M., Tajahuerce, E., and Lancis, J., "Single-pixel polarimetric imaging spectrometer by compressive sensing," *Applied Physics B* **113**(4), 551–558 (2013).

[66] Mu, T., Zhang, C., Jia, C., and Ren, W., "Static hyperspectral imaging polarimeter for full linear stokes parameters," *Optics express* **20**(16), 18194–18201 (2012).

[67] Huynh, C. P., Robles-Kelly, A., and Hancock, E., "Shape and refractive index recovery from single-view polarisation images," in [*2010 IEEE Computer Society Conference on Computer Vision and Pattern Recognition*], 1229–1236, IEEE (2010).

[68] Martin, J. A. and Gross, K. C., "Estimating index of refraction from polarimetric hyperspectral imaging measurements," *Optics express* **24**(16), 17928–17940 (2016).

[69] Atkinson, G. A. and Hancock, E. R., "Recovery of surface orientation from diffuse polarization," *IEEE transactions on image processing* **15**(6), 1653–1664 (2006).

[70] Zhao, Y.-q., Zhang, L., Zhang, D., and Pan, Q., "Object separation by polarimetric and spectral imagery fusion," *Computer Vision and Image Understanding* **113**(8), 855–866 (2009).

[71] Zhao, Y., Zhang, L., and Pan, Q., "Spectropolarimetric imaging for pathological analysis of skin," *Applied optics* **48**(10), D236–D246 (2009).

[72] Uchida, M. and Tsumura, N., "Detecting wetness on skin using rgb camera," *Journal of Imaging Science and Technology* **63**(4), 40406–1 (2019).

[73] Zhao, Y., Zhang, Q., and Yang, J., "High-resolution multiband polarization epithelial tissue imaging method by sparse representation and fusion," *Applied optics* **51**(4), A27–A35 (2012).

[74] Zhao, Y., Yang, T., Wei, P., and Pan, Q., "Spectropolarimetric imaging for skin characteristics analysis," in [*International Conference on Medical Imaging and Informatics*], 322–329, Springer (2007).

[75] Schechner, Y. Y., Narasimhan, S. G., and Nayar, S. K., "Instant dehazing of images using polarization," in [*Proceedings of the 2001 IEEE Computer Society Conference on Computer Vision and Pattern Recognition. CVPR 2001*], **1**, I–I (Dec 2001).

[76] Kocak, D. M., Dalgleish, F. R., Caimi, F. M., and Schechner, Y. Y., "A focus on recent developments and trends in underwater imaging," *Marine Technology Society Journal* **42**(1), 52–67 (2008).

[77] Homma, K., Shingu, H., Yamamoto, H., Kurosaki, H., and Shibayama, M., "Application of an imaging spectropolarimeter to agro-environmental sciences," in [*Sensors, Systems, and Next-Generation Satellites VII*], **5234**, 638–647, International Society for Optics and Photonics (2004).